

Ocean responses to Hurricane Ian from daily gap-free satellite observations

Wei Shi & Menghua Wang

To cite this article: Wei Shi & Menghua Wang (2023) Ocean responses to Hurricane Ian from daily gap-free satellite observations, Remote Sensing Letters, 14:8, 877-889, DOI: [10.1080/2150704X.2023.2247522](https://doi.org/10.1080/2150704X.2023.2247522)

To link to this article: <https://doi.org/10.1080/2150704X.2023.2247522>



© 2023 The Author(s). Published by Informa UK Limited, trading as Taylor & Francis Group.



View supplementary material [↗](#)



Published online: 24 Aug 2023.



Submit your article to this journal [↗](#)



Article views: 490



View related articles [↗](#)



View Crossmark data [↗](#)

Ocean responses to Hurricane Ian from daily gap-free satellite observations

Wei Shi^{a,b} and Menghua Wang^a

^aNOAA National Environmental Satellite, Data, and Information Service, Center for Satellite Applications and Research, College Park, MD, USA; ^bCIRA (Cooperative Institute for Research in the Atmosphere), Colorado State University, Fort Collins, CO, USA

ABSTRACT



Using gap-free satellite observations of chlorophyll-a (Chl-a) concentration, sea surface temperature (SST), and sea surface salinity (SSS) following Hurricane Ian in 2022, we demonstrate the capabilities and benefits of the collective satellite remote sensing approach to monitor the ocean physical, biological, and biogeochemical responses to a hurricane. The evolvments of Chl-a, SST, and SSS from 26 September to 7 October show that ocean responses to the hurricane are regional-specific and the spatial maps of changes in these three ocean properties are distinct. Quick SST and SSS changes were observed following the passage of Hurricane Ian, while Chl-a change lagged hurricane winds for about 3–4 days. The ocean features of the elevated Chl-a, reduced SST, and enhanced SSS after Hurricane Ian were found to last until late October 2022. Results in the temporal variations show that Chl-a more than doubled, SST dropped by $> \sim 2^\circ\text{C}$, and SSS increased by $> \sim 1$ psu in the continental shelf of the Gulf of Mexico.

ARTICLE HISTORY


Received 1 June 2023
Accepted 5 August 2023

1. Introduction

The upper ocean experiences significant physical, biological, and biogeochemical responses to a moving hurricane. Strong wind-driven vertical entrainment, upwelling and horizontal advection leads to the mixed-layer deepening and significant sea surface temperature (SST) drop along the hurricane track (Brink 1989; Price 1981; Sanford, Price, and Girton 2011). The SST drop of $\sim 2\text{--}4^\circ\text{C}$ and mixed-layer deepening of ~ 80 m have been documented (Monaldo et al. 1997; Sanford, Price, and Girton 2011; Shi and Wang 2007). Anomalous SST along the hurricane track can last $\sim 5\text{--}15$ days (Price 1981; Price, Morzel, and Niiler 2008). The SST response to the hurricane is also rightward biased (Price 1981; Shi and Wang 2011). It is also found that pre-existing oceanic conditions are closely associated with the responses of the upper ocean to a hurricane (Liu, Wang, and Shi 2009; Walker, Leben, and Balasubramanian 2005; Zheng, Ho, and Kuo 2008).

CONTACT Wei Shi  wei.1.shi@noaa.gov  NOAA National Environmental Satellite, Data, and Information Service, Center for Satellite Applications and Research, E/RA3, 5830 University Research Ct, College Park, MD, USA

This article has been republished with minor changes. These changes do not impact the academic content of the article.

 Supplemental data for this article can be accessed online at <https://doi.org/10.1080/2150704X.2023.2247522>.

© 2023 The Author(s). Published by Informa UK Limited, trading as Taylor & Francis Group.

This is an Open Access article distributed under the terms of the Creative Commons Attribution License (<http://creativecommons.org/licenses/by/4.0/>), which permits unrestricted use, distribution, and reproduction in any medium, provided the original work is properly cited. The terms on which this article has been published allow the posting of the Accepted Manuscript in a repository by the author(s) or with their consent.

The hurricane-driven mixed-layer deepening by entrainment and upwelling not only dramatically changes the vertical profiles of ocean temperature but also alters the profiles of salinity and nutrient, as well as sediment concentration. Salinity in the upper ocean increases after the initial salinity profile shows a fresher surface layer (Gierach, Subrahmanyam, and Thoppil 2009; Prasad and Hogan 2007; Sanford, Price, and Girton 2011). There was an overall increase in nitrate levels in the upper 50 m from a pre-storm value of $\sim 3.2 \mu\text{M}$ to a post-storm value of $\sim 4.7 \mu\text{M}$ following Hurricane Katrina (Gierach, Subrahmanyam, and Thoppil 2009). The shallow nutricline at about 50 m and a sharp increase in nitrate concentration were reported following the tropical cyclone Kai-Tak (Lin et al. 2003). Satellite observations from the Cloud-Aerosol Lidar and Infrared Pathfinder Satellite Observations (CALIPSO) also show sediment vertical profile became relatively uniform in the upper 50 m depth after Cyclone Nargis (Shi and Wang 2008).

Due to its capability for large-scale and high temporal observations, satellite remote sensing has been widely used to monitor the ocean environment response to hurricanes. Satellite imagery of SST cooling has been reported with a variety of hurricanes (Monaldo et al. 1997; Stramma, Cornillon, and Price 1986). Remotely sensed ocean colour data show the increase in post-storm surface chlorophyll-a (Chl-a) concentration within the cool wakes for $\sim 2\text{--}3$ weeks (Babin et al. 2004). In fact, Chl-a could increase by over 10 folds with a time lag of ~ 4 days following Hurricane Katrina (Gierach and Subrahmanyam 2007; Shi and Wang 2007). Cyclone Kai-Tak triggered an average of 30-fold increase in ocean surface Chl-a, and carbon fixation and primary production were estimated to be ~ 0.8 Mt from measurements of the Sea-viewing Wide Field-of-view Sensor (SeaWiFS) (Lin et al. 2003). Enhanced sediment concentration and coloured dissolved organic matter (CDOM) were also reported following the passage of a hurricane or a tropical storm from satellite ocean colour observations (Hoge and Lyon 2002; Hu and Muller-Karger 2007; Shi and Wang 2008).

Decade-long satellite sea surface salinity (SSS) observations show that the initial rain-induced dilution of the salinity is quickly dominated by the saltier water entrainment and leads to surface salinification of ~ 0.3 psu for the most intense storms. This is attributed to the vertical salinity gradient in the upper ocean (Reul et al. 2021). Another study from satellite observations also shows that salinification is larger on the right (left)-hand side of the storm motion in the Northern (Southern) Hemisphere, consistent with the location of stronger turbulent mixing, and stronger tropical cyclones tend to produce longer-lasting, stronger, and deeper salinification (Sun, Vecchi, and Soden 2021).

Even though there are already numerous efforts in applying satellite observations, e.g., Chl-a, SST, SSS, to study the ocean's physical, biological, and biogeochemical responses to hurricanes, most of the studies were focused only on one specific ocean property, but responses of the ocean environment to a hurricane are multi-faceted. These responses involve a variety of atmospheric and ocean's physical, optical, biological, and biogeochemical processes. On the other hand, the availability of satellite observations is often intermittent with some data gaps between satellite overpasses. As an example, normally there are no valid Chl-a data from satellite observations in a couple of days before and after the hurricane passage due to cloud coverage.

In this study, daily gap-free Chl-a (Wang and Son 2016) and diffuse attenuation coefficients at 490 nm ($K_d(490)$) (Wang, Son, and Harding 2009) using the Data Interpolating Empirical Orthogonal Functions (DINEOF) from the Visible Infrared

Imaging Radiometer Suite (VIIRS) observations (Liu and Wang 2018, 2022), daily gap-free NOAA high-resolution blended SST using multi-satellite sensor data with the Optimum Interpolation (OI) technique (Reynolds et al. 2007), and daily 8-day-running-mean SSS measurements from the Soil Moisture Active Passive (SMAP) mission (Fore et al. 2016) are used to study the physical, biological, and biogeochemical responses to Hurricane Ian. It is noted that, with a swath of 1000 km, it takes SMAP approximately 3 days to complete global coverage with a repeat cycle of 8 days. The daily SMAP SSS product is produced using the 8-day measurements to resample onto a 0.25° fixed Earth grid using the OI algorithm. The SMAP SSS data have an accuracy of ~ 0.2 psu in comparison to the in situ measurements (Tang et al. 2017)

VIIRS ocean colour products including normalized water-leaving radiance ($nL_w(\lambda)$) spectra and Chl-a have been routinely monitored and validated using in situ measurements such as the Marine Optical Buoy (MOBY) in waters off Hawaii (Clark et al. 1997), the Aerosol Robotic Network Ocean Colour (AERONET-OC) data (Zibordi et al. 2009), and annual dedicated VIIRS calibration and validation (Cal/Val) cruise measurements, e.g., see a recent cruise report (Ondrusek et al. 2022). It is noted that VIIRS Chl-a data have been generated using the ocean colour index (OCI) algorithm, which has been shown to generally produce reliable and accurate Chl-a over global open oceans (Hu, Lee, and Franz 2012; O'Reilly and Werdell 2019; Wang and Son 2016). Studies show that VIIRS daily gap-free Chl-a data have an accuracy similar to the original data (Liu and Wang 2019, 2022, 2023). In fact, results show that the Chl-a differences between gap-filled and original data are usually within ~ 1 – 2% (Liu and Wang 2019, 2022). There could be some significant and quick changes such as the resuspension of sediments or storm surge in the offshore optically shallow waters when a hurricane with strong winds passes across. However, the region in this study is dominantly optically deep waters. Thus, VIIRS-observed data gaps over a hurricane are essentially the same as those caused by the cloud coverage. Gap-free satellite ocean colour data can indeed capture ocean variability before, during, and after the hurricane in the entire study region, even though the rapid extreme water property changes in the optically shallow waters during the hurricane passage might be missed.

The objective of this study is two-fold. First, we demonstrate a collective approach to monitor the overall ocean physical, biological, and biogeochemical responses to Hurricane Ian using the available satellite observations. On the other hand, the gap-free data will further reveal the ocean environmental changes and their status before and after the passage of the hurricane. Second, using these satellite measurements, we can then characterize and understand various relationships and inter-dependence of ocean physical, biological, and biogeochemical processes driven by a hurricane.

2. Ocean environmental changes with Hurricane Ian

As the second major hurricane in the 2022 Atlantic hurricane season, Hurricane Ian (Figure 1) caused widespread damage across Cuba, and the US states of Florida, South Carolina, and North Carolina. It originated off the west coast of Africa and further developed as a tropical depression in the Caribbean, then became a Tropical Storm Ian on 24 September 2022. On 27 September 2022, it made landfall in Cuba as a category 3 hurricane with the sustained winds of ~ 205 km hour⁻¹. After crossing the Gulf of Mexico, it strengthened as a category 4 hurricane. Hurricane Ian made its first and second landfalls

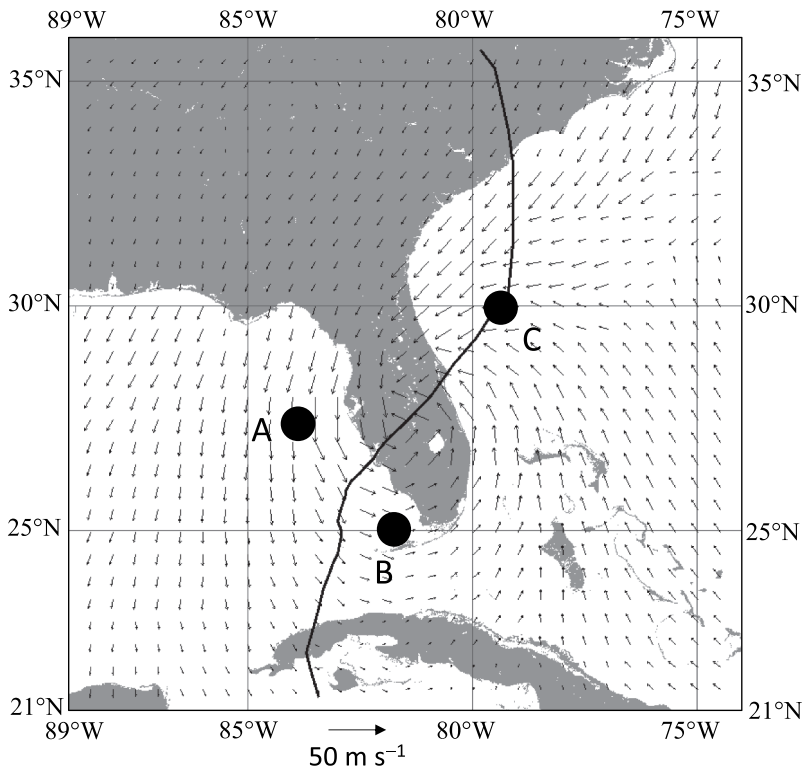


Figure 1. Snapshot of Hurricane Ian wind fields at 6:00 UTC on 29 September 2022, with the track of Hurricane Ian overlaid in solid line. The pseudo stations A located at [27.2°N, 84.0°W], B at [25.0°N, 81.8°W], and C [30.0°N, 79.4°W] are marked with solid dark circles for further analysis.

at 19:05 UTC and 20:35 UTC, respectively, in Florida on 28 September 2022. The hurricane crossed Florida and moved north-northeast off the eastern Florida as a tropical storm with weakened strength. In the offshore region, it further strengthened to a Category 1 hurricane and moved northward. It made its third landfall in South Carolina at ~18:00 UTC on 30 September 2022, with sustained winds of 130 km hour^{-1} . After making its third landfall, it quickly weakened and became a post-tropical cyclone. It eventually dissipated on 1 October 2022, in the central North Carolina.

2.1. *Chl-a changes between 26 September and 7 October*

Using Chl-a as a representative parameter, Figure 2 shows the biological variation in the vast region Hurricane Ian passed and impacted. On 26 September, Hurricane Ian was still located in the Caribbean Sea. The difference between the Chl-a distribution before 26 September and that on 26 September was trivial. Thus, Chl-a on 26 September is used as a reference to characterize Chl-a changes following the passage of Hurricane Ian.

On 27 September, the change of Chl-a in the entire region was not noticeable (Figure 2 (b,f)). On 28 September (Figure 2(c)) and 29 September (Figure 2(d)), the Chl-a spatial pattern was still similar to that on 26 September (Figure 2(a)) when Hurricane Ian crossed Florida. On the other hand, the patterns of both moderately enhanced and decreased Chl-

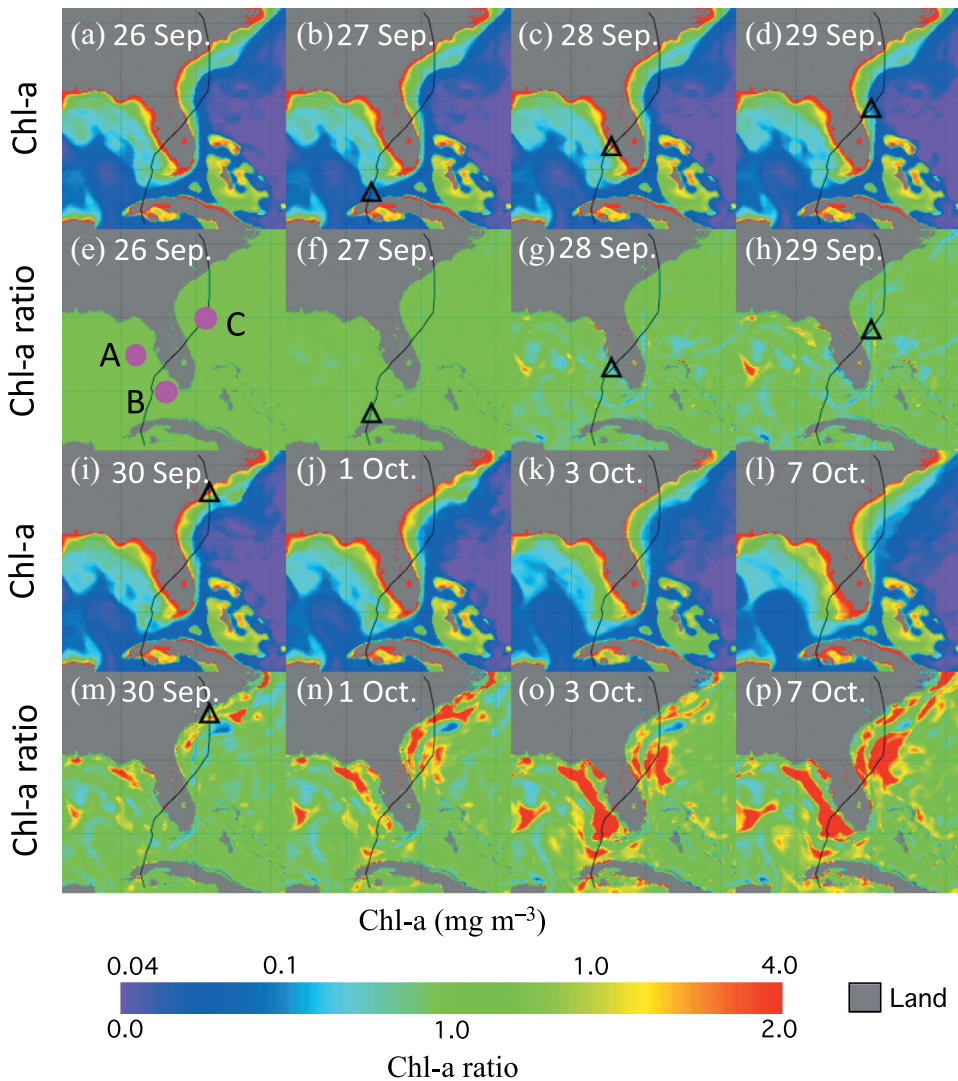


Figure 2. Chl-a and Chl-a ratio (between daily Chl-a and Chl-a on 26 September) on (a, e) 26 September, (b, f) 27 September, (c, g) 28 September, (d, h) 29 September, (i, m) 30 September, (j, n) 1 October, (k, o) 3 October, and (l, p) 7 October. Note that the hurricane track is overlaid in each panel with the hurricane eye location at 18:00 UTC on that day marked in black triangle.

a were found in the Gulf of Mexico (Figure 2(g,h)). On 30 September, noticeable change of Chl-a from the previous day could be found in the Gulf of Mexico, while the change of Chl-a along the southern Atlantic coast started to be obvious (Figure 2(m)).

From 1 October (Figure 2(j)), a long band of the enhanced Chl-a along the western Florida coastal region developed 4 days after Hurricane Ian passed this region (Figure 2(n)). In the continental shelf region off the southern Atlantic coast, several patches of the enhanced Chl-a were also observed. This might reflect the effect of the interaction between Hurricane Ian and the Gulf Stream (Ezer 2018). On 3 October (Figure 2(k,o)) and 7 October (Figure 2(i,p)), the enhanced Chl-a further strengthened, and the

patterns of enhanced Chl-a expanded to cover more area in the Gulf of Mexico and the continental shelf off the US southeastern coast.

Figure S1 shows the changes of $K_d(490)$. The change of $K_d(490)$ (measure of water turbidity) (Wang, Son, and Harding 2009) is more sensitive than Chl-a even though the spatial patterns of $K_d(490)$ and Chl-a are similar due to the intrinsic relationship between Chl-a and $K_d(490)$ (Morel et al. 2007). Notably, the $K_d(490)$ ratio (between daily $K_d(490)$ and $K_d(490)$ on 26 September) on 30 September (Figure S1(m)) already showed the $K_d(490)$ changes and the spatial patterns of $K_d(490)$ from 1–7 October (Figure S1(j–l)) were significantly different from those on 26 September, while these changes are not clear for Chl-a in Figure 2. On the other hand, $K_d(490)$ clearly showed the significant impact of Hurricane Ian on the water turbidity within the Outer Banks before (Figure S1(h,m)) and after (Figure S1(n,o)) the hurricane approached this region on 30 September.

2.2. SST changes between 26 September and 7 October

Hurricane Ian led to a broad drop of SST in the Gulf of Mexico and continental shelf region along the US southeast Atlantic coast. A noticeable SST drop started on 28 September when Hurricane Ian landed along the Florida southwestern coast (Figure 3(c,g)). SST further dropped and the area of decreased SST expanded as the hurricane crossed Florida (Figure 3(d,h)) on 29 September, and landed in South Carolina (Figure 3(i, m)) on 30 September. In the period from 1–7 October, SST further decreased in the Gulf of Mexico (Figure 3(j–l)). In the most part of the northern Gulf of Mexico, SST were $<26^\circ\text{C}$ (Figure 3(l)) and a drop of up to $\sim 2^\circ\text{C}$ in SST occurred. On 7 October, a significant SST drop in the offshore region of South Carolina was observed (Figure 3(l,p)) in comparison to the SST map 4 days ago on 3 October (Figure 3(k,o)). The broad SST drop in the study region can be attributed to the enhanced vertical mixing, entrainment, and upwelling driven by the strong hurricane winds.

2.3. SSS changes between 26 September and 7 October

As an ocean physical property, the SSS is usually significantly impacted by a passing hurricane. Therefore, a broad response of SSS was observed after the passage of Hurricane Ian (Figure 4). However, the change of SSS was different from that of SST as shown in Figure 3. In comparison to the gradual SST response, a significant response of SSS to Hurricane Ian was observed immediately after the hurricane passage. On 28 September (Figure 4(c,g)), SSS began to increase in the northern Gulf of Mexico. In fact, SSS in a large area of the northern Gulf of Mexico were $> \sim 0.5$ psu higher on 29 September (Figure 4(d, h)) than those of 3 days ago on 26 September (Figure 4(a)). This implies that the halocline depth was shallow in this region due to the freshwater inflow from the Mississippi River. Like the SST change following Hurricane Ian, strong wind-induced ocean processes such as the enhanced vertical mixing and upwelling brought the salty sub-surface water to the surface and led to a broad increase in SSS following the passage of the hurricane.

Continuous increases in SSS were observed after 30 September (Figure 4(i,m)). The SSS increase spreads broadly to the continental shelf of the Gulf of Mexico (Figure 4(n–p)). Moderate decrease of SSS was also shown in the central Gulf of Mexico during this period (Figure 4(m–p)). In the offshore region off the Georgia

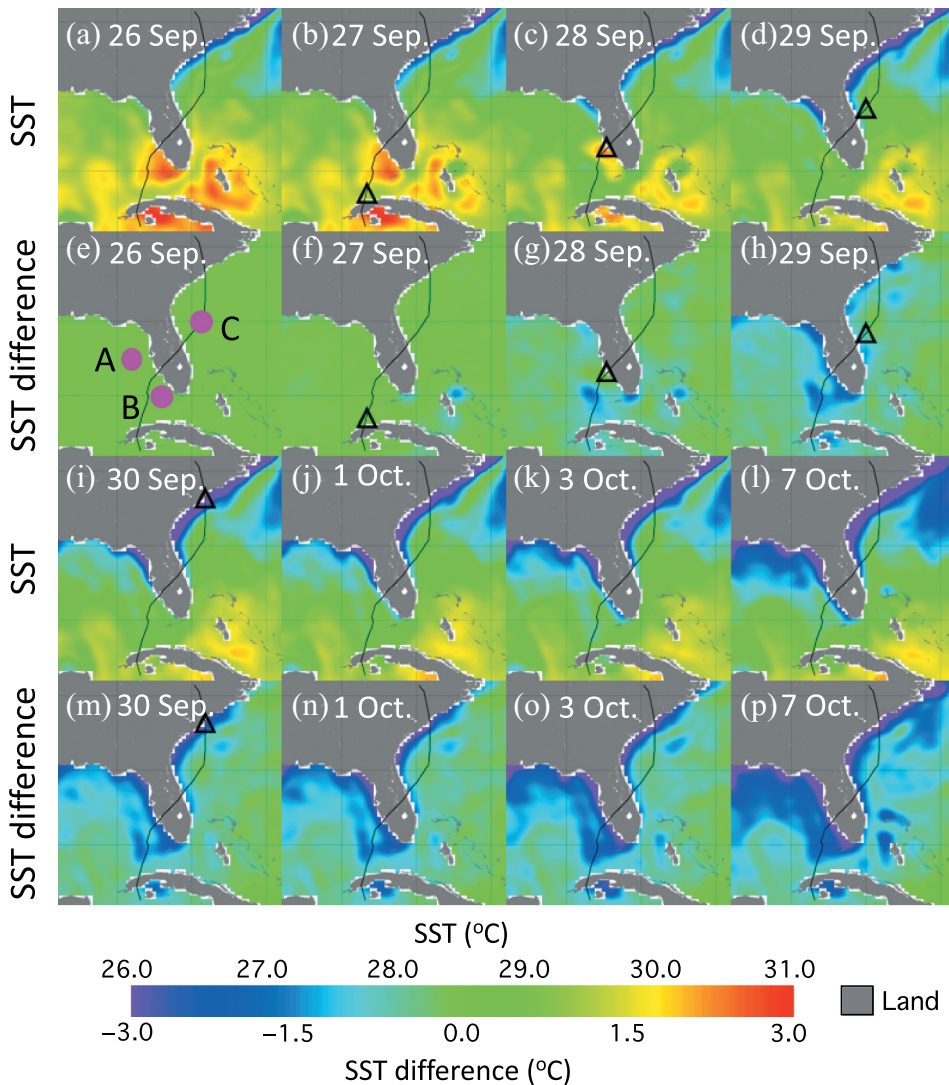


Figure 3. SST and SST difference (between daily SST and SST on 26 September) on (a, e) 26 September, (b, f) 27 September, (c, g) 28 September, (d, h) 29 September, (i, m) 30 September, (j, n) 1 October, (k, o) 3 October, and (l, p) 7 October. Note that the hurricane track is overlaid in each panel with the hurricane eye location at 18:00 UTC on that day marked in dark triangle.

coast at about (30°N, 80°W), SSS dropped by over ~0.5 psu on 30 September (Figure 4(m)) and 1 October (Figure 4(n)). Further examination of the sea surface height (SSH) product (not shown here) suggests that this might be caused by a sub-mesoscale filament feature related to the Gulf Stream (Ezer 2018). On 7 October, enhanced SSS was observed in the offshore region of South Carolina (Figure 4(p)). This is consistent with the decreased SST in this region on the same date as shown in (Figure 3(p)).

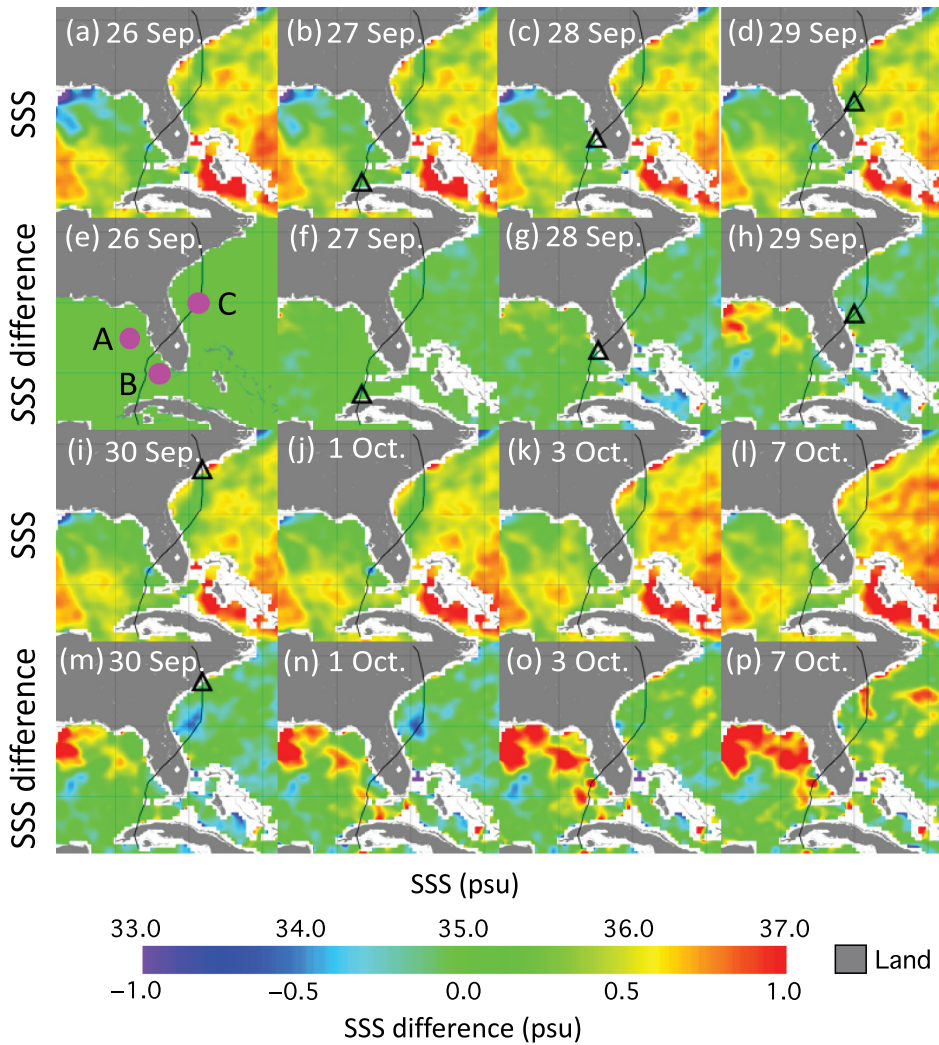


Figure 4. SSS and SSS difference (between daily SSS and SSS on 26 September) on (a, e) 26 September, (b, f) 27 September, (c, g) 28 September, (d, h) 29 September, (i, m) 30 September, (j, n) 1 October, (k, o) 3 October, and (l, p) 7 October. Note that the hurricane track is overlaid in each panel with the hurricane eye location at 18:00 UTC on that day marked in dark triangle.

3. Quantitative evaluations

It is well known that it is extremely difficult and dangerous to acquire in situ measurements during hurricane conditions. There were also no in situ data available in the Gulf of Mexico to further validate the satellite retrievals. The AERONET-OC WaveCIS site also stopped working since May 2022. To further characterize the ocean environmental response to Hurricane Ian, three pseudo-stations in the Gulf of Mexico (station A), near Florida key region (station B), and in the South Atlantic Bight (station C) were selected (see Figures 1,2(e)–4(e)). The selection of these three pseudo-stations in the Gulf of Mexico, Loop Current and Gulf Stream, and South

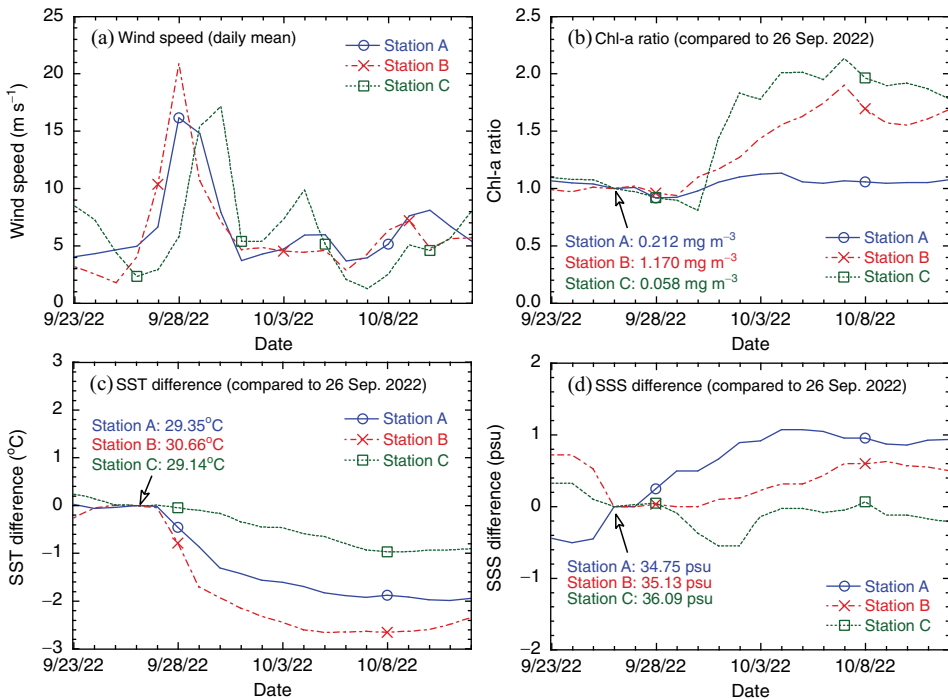


Figure 5. Time series at stations A, B, and C between 23 September and 12 October for (a) daily mean wind speed, (b) Chl-a ratio, (c) SST difference, and (d) SSS difference. Note that Chl-a, SST, and SSS values on 26 September at the three stations are noted in plots (b)–(d) and they were used as the corresponding references.

Atlantic Bight can well represent the study region affected by Hurricane Ian. Figure 5(a) shows that the mean daily wind speeds reached the maximum $\sim 16 \text{ m s}^{-1}$ at station A on 28 September, $\sim 22 \text{ m s}^{-1}$ at station B on 28 September, and $\sim 17 \text{ m s}^{-1}$ at station C on 30 September. The intensified wind lasted about 3–4 days at these stations Figure 5(a).

Significant Chl-a changes occurred at stations B and C, while the Chl-a variation at station A was relatively less significant (Figures 5(b) and S2). For all these stations, the variations of ocean properties before 26 September were trivial. At station A, the Chl-a ratio increased to ~ 1.13 (Chl-a difference of 0.028 mg m^{-3}) on 4 October after an initial slight Chl-a drop. At station B, Chl-a monotonously increased until 7 October with Chl-a ratio of ~ 1.90 (Chl-a difference of 1.055 mg m^{-3}), and then it remained elevated in mid-October for over about two weeks after the hurricane passed this site. At station C, Chl-a ratio showed a quick increase after the peak hurricane wind on 30 September. On 2 October, the Chl-a ratio at station C was ~ 1.83 (Chl-a difference of 0.048 mg m^{-3}). The enhanced Chl-a at station C persisted for more than 2 weeks. On 12 October, Chl-a were still well above the pre-hurricane values with a Chl-a ratio of ~ 1.78 (Chl-a difference of 0.045 mg m^{-3}).

The time series of $K_d(490)$ at stations A, B, and C (Figure S3) show that significant $K_d(490)$ changes occurred at station B. $K_d(490)$ at station B increased from $< \sim 0.15 \text{ m}^{-1}$ before Hurricane Ian to $\sim 0.52 \text{ m}^{-1}$ on 1 October (Figure S3(a)). Moderate changes of K_d

(490) occurred at station C with $K_d(490)$ ratio reaching ~ 1.26 on 6 October (Figure S3(b)). There was little change of $K_d(490)$ at station A before and after the passage of Hurricane Ian.

At these three stations, SST showed immediate decreases as the hurricane approached the study region. At stations A and B, notable SST drops happened when Hurricane Ian was in the Gulf of Mexico, and it was in phase with the maximum winds in the period between 27–30 September (Figure 5(a)). Specifically, on 5 October, the SST difference reached $\sim -1.82^\circ\text{C}$ and $\sim -2.66^\circ\text{C}$ at stations A and B (Figure 5(c)), respectively. In fact, the reduced SST lasted until mid-October and was still significant at the end of October. At station C, SST showed a slow drop from 28 September to 8 October, and SST was lower by $\sim 1.0^\circ\text{C}$ on 8 October than the pre-hurricane SST values.

Hurricane Ian led to a gradual increase in SSS at stations A and B (Figure 5(d)). In general, the SSS changes at stations A and B were more significant than that at station C. On 4 October, SSS was ~ 1.07 psu higher than that on 26 September at station A. The SSS increase was less significant at station B than that at station A, and their difference at station B reached ~ 0.6 psu on 7 October. In comparison to SSS at stations A and B, SSS at station C were relatively stable in the entire period between 28 September and mid-October. The quick SSS drop of ~ 0.6 psu in early October might be attributed to the ocean filament features associated with the Gulf Stream (Ezer 2018).

Summary

In this study, we use daily gap-free Chl-a, SST, and SSS data to demonstrate that satellite observations can be used as effective tools to monitor and characterize ocean physical, biological, and biogeochemical changes following the passage of Hurricane Ian. Multi-satellite measurements of these ocean properties are critical for us to better understand various ocean processes and their interactions in the ocean-atmosphere system after the passage of a hurricane. Results show that the responses of these ocean properties (Chl-a, SST, and SSS) to Hurricane Ian were not the same in terms of both the spatial distributions and temporal variations. This suggests that the pre-hurricane ocean conditions such as the vertical profiles of the ocean temperature, salinity, and nutrients, the existence of the ocean current, eddies, ocean fronts, etc., also played important roles in determining the corresponding changes of Chl-a, SST, and SSS. This study also shows that the daily gap-free satellite data are useful to have detailed high temporal monitoring of various ocean property variations and responses to natural events (e.g., hurricanes, large blooms, etc.). Furthermore, multi-satellite gap-free product data can help the modelling effort to assess the ocean's dynamics that drives the physical, optical, biological, and biogeochemical changes and eventually forecast/nowcast the ocean environmental variations following the passage of a hurricane.

Acknowledgments

We thank two anonymous reviewers for their useful comments. The scientific results and conclusions, as well as any views or opinions expressed herein, are those of the author(s) and do not necessarily reflect those of NOAA or the Department of Commerce.

Disclosure statement

No potential conflict of interest was reported by the author(s).

Funding

This research was supported by the Joint Polar Satellite System (JPSS) funding. VIIRS global ocean color product data, as well as product monitoring and validation results, can be found at the NOAA Ocean Color Science Team website (<https://www.star.nesdis.noaa.gov/sod/mecb/color/>). The SMAP SSS data were acquired from Jet Propulsion Laboratory (JPL) Physical Oceanography Distribution Active Archive Center (PODAAC) (<https://doi.org/10.5067/SMP50-3TPCS>). The SST data were obtained from NOAA Physical Science Laboratory (<https://psl.noaa.gov/>).

References

- Babin, S. M., J. A. Carton, T. D. Dickey, and J. D. Wiggert. 2004. "Satellite Evidence of Hurricane-Induced Phytoplankton Blooms in an Oceanic Desert." *Journal of Geophysical Research-Oceans* 109 (C3): Artn C03043. <https://doi.org/10.1029/2003jc001938>.
- Brink, K. H. 1989. "Observations of the Response of Thermocline Currents to a Hurricane." *Journal of Physical Oceanography* 19:1017–1022. [https://doi.org/10.1175/1520-0485\(1989\)019<1017:Ootrot>2.0.Co;2](https://doi.org/10.1175/1520-0485(1989)019<1017:Ootrot>2.0.Co;2).
- Clark, D. K., H. R. Gordon, K. J. Voss, Y. Ge, W. Broenkow, and C. Trees. 1997. "Validation of Atmospheric Correction Over the Oceans." *Journal of Geophysical Research-Atmospheres* 102 (D14): 17209–17217. <https://doi.org/10.1029/96jd03345>.
- Ezer, T. 2018. "On the Interaction Between a Hurricane, the Gulf Stream and Coastal Sea Level." *Ocean Dynamics* 68:1259–1272. <https://doi.org/10.1007/s10236-018-1193-1>.
- Fore, A. G., S. H. Yueh, W. Q. Tang, B. W. Stiles, and A. K. Hayashi. 2016. "Combined Active/Passive Retrievals of Ocean Vector Wind and Sea Surface Salinity with SMAP." *IEEE Transactions on Geoscience & Remote Sensing* 54:7396–7404. <https://doi.org/10.1109/Tgrs.2016.2601486>.
- Gierach, M. M., and B. Subrahmanyam. 2007. "Satellite Data Analysis of the Upper Ocean Response to Hurricanes Katrina and Rita (2005) in the Gulf of Mexico." *IEEE Geoscience and Remote Sensing Letters* 4 (1): 132–136. <https://doi.org/10.1109/Lgrs.2006.887145>.
- Gierach, M. M., B. Subrahmanyam, and P. G. Thoppil. 2009. "Physical and Biological Responses to Hurricane Katrina (2005) in a 1/25° Nested Gulf of Mexico HYCOM." *Journal of Marine Systems* 78 (1): 168–179. <https://doi.org/10.1016/j.jmarsys.2009.05.002>.
- Hoge, F. E., and P. E. Lyon. 2002. "Satellite Observation of Chromophoric Dissolved Organic Matter (CDOM) Variability in the Wake of Hurricanes and Typhoons." *Geophysical Research Letters* 29 (19): 14-1-14-4. Artn 1908. <https://doi.org/10.1029/2002gl015114>.
- Hu, C., Z. Lee, and B. Franz. 2012. "Chlorophyll a Algorithms for Oligotrophic Oceans: A Novel Approach Based on Three-Band Reflectance Difference." *Journal of Geophysical Research-Oceans* 117 (C1). <https://doi.org/10.1029/2011jc007395>.
- Hu, C. M., and F. E. Muller-Karger. 2007. "Response of Sea Surface Properties to Hurricane Dennis in the Eastern Gulf of Mexico." *Geophysical Research Letters* 34 (7). <https://doi.org/10.1029/2006GL028935>.
- Lin, I., W. T. Liu, C. C. Wu, G. T. F. Wong, C. M. Hu, Z. Q. Chen, W. D. Liang, Y. Yang, and K. K. Liu. 2003. "New Evidence for Enhanced Ocean Primary Production Triggered by Tropical Cyclone." *Geophysical Research Letters* 30 (13): Artn 1718. <https://doi.org/10.1029/2003gl017141>.
- Liu, X., and M. Wang. 2018. "Gap Filling of Missing Data for VIIRS Global Ocean Color Products Using the DINEOF Method." *IEEE Transactions on Geoscience & Remote Sensing* 56 (8): 4464–4476. <https://doi.org/10.1109/Tgrs.2018.2820423>.

- Liu, X., and M. Wang. 2019. "Filling the Gaps of Missing Data in the Merged VIIRS SNPP/NOAA-20 Ocean Color Product Using the DINEOF Method." *Remote Sensing* 11 (2): 178. <https://doi.org/10.3390/rs11020178>.
- Liu, X., and M. Wang. 2022. "Global Daily Gap-Free Ocean Color Products from Multi-Satellite Measurements." *International Journal of Applied Earth Observation and Geoinformation* 108:102714. <https://doi.org/10.1016/j.jag.2022.102714>.
- Liu, X., and M. Wang. 2023. "High Spatial Resolution Gap-Free Global and Regional Ocean Color Products." *IEEE Transactions on Geoscience and Remote Sensing: A Publication of the IEEE Geoscience and Remote Sensing Society* 61:1–18. <https://doi.org/10.1109/tgrs.2023.3271465>.
- Liu, X., M. Wang, and W. Shi. 2009. "A Study of a Hurricane Katrina-Induced Phytoplankton Bloom Using Satellite Observations and Model Simulations." *Journal of Geophysical Research-Oceans* 114 (C3): Artn C03023. <https://doi.org/10.1029/2008jc004934>.
- Monaldo, F. M., T. D. Sikora, S. M. Babin, and R. E. Sterner. 1997. "Satellite Imagery of Sea Surface Temperature Cooling in the Wake of Hurricane Edouard (1996)." *Monthly Weather Review* 125:2716–2721. [https://doi.org/10.1175/1520-0493\(1997\)125<2716:Siosst>2.0.Co;2](https://doi.org/10.1175/1520-0493(1997)125<2716:Siosst>2.0.Co;2).
- Morel, A., Y. Huot, B. Gentili, P. J. Werdell, S. B. Hooker, and B. A. Franz. 2007. "Examining the Consistency of Products Derived from Various Ocean Color Sensors in Open Ocean (Case 1) Waters in the Perspective of a Multi-Sensor Approach." *Remote Sensing of Environment* 111 (1): 69–88. <https://doi.org/10.1016/j.rse.2007.03.012>.
- Ondrusek, M., M. Wang, E. Stengel, C. Kovach, A. Gilerson, E. Herrera, M. Malinowski, et al. 2022. *Report for Dedicated JPSS VIIRS Ocean Color Calibration/Validation Cruise: Gulf of Mexico in April 2021*. edited by Wei J. NOAA Technical Report NESDIS 157. Silver Spring, Maryland, USA: NOAA National Environmental Satellite, Data, and Information Service. <https://doi.org/10.25923/x2q6-9418>.
- O'Reilly, J. E., and P. J. Werdell. 2019. "Chlorophyll Algorithms for Ocean Color Sensors-OC4, OC5 & OC6." *Remote Sensing of Environment* 229:32–47. <https://doi.org/10.1016/j.rse.2019.04.021>.
- Prasad, T. G., and P. J. Hogan. 2007. "Upper-Ocean Response to Hurricane Ivan in a 1/25° Nested Gulf of Mexico HYCOM." *Journal of Geophysical Research-Oceans* 112(C4). Artn C04013. <https://doi.org/10.1029/2006JC003695>.
- Price, J. F. 1981. "Upper Ocean Response to a Hurricane." *Journal of Physical Oceanography* 11:153–175. [https://doi.org/10.1175/1520-0485\(1981\)011<0153:Uortah>2.0.Co;2](https://doi.org/10.1175/1520-0485(1981)011<0153:Uortah>2.0.Co;2).
- Price, J. F., J. Morzel, and P. P. Niiler. 2008. "Warming of SST in the Cool Wake of a Moving Hurricane." *Journal of Geophysical Research-Oceans* 113 (C7): Artn C07010. <https://doi.org/10.1029/2007JC004393>.
- Reul, N., B. Chapron, S. A. Grodsky, S. Guimbard, V. Kudryavtsev, G. R. Foltz, and K. Balaguru. 2021. "Satellite Observations of the Sea Surface Salinity Response to Tropical Cyclones." *Geophysical Research Letters* 48 (1): ARTN e2020GL091478. <https://doi.org/10.1029/2020GL091478>.
- Reynolds, R. W., T. M. Smith, C. Liu, D. B. Chelton, K. S. Casey, and M. G. Schlax. 2007. "Daily High-Resolution-Blended Analyses for Sea Surface Temperature." *Journal of Climate* 20 (22): 5473–5496. <https://doi.org/10.1175/2007jcli1824.1>.
- Sanford, T. B., J. F. Price, and J. B. Girton. 2011. "Upper-Ocean Response to Hurricane Frances (2004) Observed by Profiling EM-APEX Floats." *Journal of Physical Oceanography* 41 (6): 1041–1056. <https://doi.org/10.1175/2010jpo4313.1>.
- Shi, W., and M. Wang. 2007. "Observations of a Hurricane Katrina-Induced Phytoplankton Bloom in the Gulf of Mexico." *Geophysical Research Letters* 34 (11): Artn L11607. <https://doi.org/10.1029/2007gl029724>.
- Shi, W., and M. Wang. 2008. "Three-Dimensional Observations from MODIS and CALIPSO for Ocean Responses to Cyclone Nargis in the Gulf of Martaban." *Geophysical Research Letters* 35 (21): Artn L21603. <https://doi.org/10.1029/2008GL035279>.
- Shi, W., and M. H. Wang. 2011. "Satellite Observations of Asymmetrical Physical and Biological Responses to Hurricane Earl." *Geophysical Research Letters* 38 (4): Artn L04607. <https://doi.org/10.1029/2010GL046574>.
- Stramma, L., P. Cornillon, and J. F. Price. 1986. "Satellite-Observations of Sea-Surface Cooling by Hurricanes." *Journal of Geophysical Research-Oceans* 91 (C4): 5031–5035. <https://doi.org/10.1029/JC091iC04p05031>.

- Sun, J. R., G. Vecchi, and B. Soden. 2021. "Sea Surface Salinity Response to Tropical Cyclones Based on Satellite Observations." *Remote Sensing* 13. ARTN 420. <https://doi.org/10.3390/rs13030420>.
- Tang, W. Q., A. Fore, S. Yueh, T. Lee, A. Hayashi, A. Sanchez-Franks, J. Martinez, B. King, and D. Baranowski. 2017. "Validating SMAP SSS with in situ Measurements." *Remote Sensing of Environment* 200:326–340. <https://doi.org/10.1016/j.rse.2017.08.021>.
- Walker, N. D., R. R. Leben, and S. Balasubramanian. 2005. "Hurricane-Forced Upwelling and Chlorophyll a Enhancement within Cold-Core Cyclones in the Gulf of Mexico." *Geophysical Research Letters* 32 (18). <https://doi.org/10.1029/2005GL023716>.
- Wang, M., and S. Son. 2016. "VIIRS-Derived Chlorophyll-A Using the Ocean Color Index Method." *Remote Sensing of Environment* 182:141–149. <https://doi.org/10.1016/j.rse.2016.05.001>.
- Wang, M., S. Son, and L. W. Harding. 2009. "Retrieval of Diffuse Attenuation Coefficient in the Chesapeake Bay and Turbid Ocean Regions for Satellite Ocean Color Applications." *Journal of Geophysical Research-Oceans* 114 114 (C10): Artn C10011. <https://doi.org/10.1029/2009jc005286>.
- Zheng, Z. W., C. R. Ho, and N. J. Kuo. 2008. "Importance of Pre-Existing Oceanic Conditions to Upper Ocean Response Induced by Super Typhoon Hai-Tang." *Geophysical Research Letters* 35 (20): Artn L20603. <https://doi.org/10.1029/2008GL035524>.
- Zibordi, G., B. Giles, I. D'Alimonte, D. Holben, D. Slutsker, F. Melin, J. F. Berthon, et al. 2009. "AERONET-OC: A Network for the Validation of Ocean Color Primary Products." *Journal of Atmospheric and Oceanic Technology* 26 (8): 1634–1651. <https://doi.org/10.1175/2009jtecho654.1>.